RSC Advances

PAPER

View Article Online
View Journal | View Issue

CrossMark click for updates

Cite this: *RSC Adv.*, 2015, **5**, 32159

High-performance supercapacitors based on novel carbons derived from *Sterculia lychnophora*

Xu Zhang, Chao Peng, Ru-tao Wang and Jun-wei Lang*

In this paper, two nanoporous carbons were prepared from *Sterculia lychnophora* (SL) by simple hydrothermal conditions followed by a KOH activation step with and without a carbonization process. Structural characterization indicates that the carbon sample without the carbonization process (AC-1) exhibits a cross linked and hole-like structure, a BET surface area of 2589 $m^2\ g^{-1}$, pore volume of 1.21 $cm^3\ g^{-1}$ and BJH average pore width of 2.78 nm. The carbon sample with the carbonization process (AC-2) shows dozens of nanometer microspheres, a BET surface area of 2660 $m^2\ g^{-1}$, pore volume of 1.258 $cm^3\ g^{-1}$ and BJH average pore width of 3.321 nm. The electrochemical capacitance behaviors of these carbon materials were investigated in KOH and $NaNO_3$ aqueous solutions in three and two-electrode cells, respectively. By using the $NaNO_3$ electrolyte, the efficient capacitor can work in a wider voltage window of 1.7 V without any significant capacitance fading over 3000 cycles; the highest specific capacitance of 47.8 F g^{-1} and energy density of 18.5 W h kg^{-1} are demonstrated. The desirable porous structure and electrochemical characteristics may enable SL biomass based carbon to be excellent electrode materials for high performance electrical energy storage devices.

Received 3rd February 2015
Accepted 30th March 2015

DOI: 10.1039/c5ra02085a

www.rsc.org/advances

Published on 30 March 2015. Downloaded by Michigan State University on 25/01/2016 01:14:11.

1 Introduction

With the increasing demand for supercapacitors in portable electronic devices and hybrid electric vehicles, the components of supercapacitors, such as electrode materials, electrolyte and separator membrane have been research emphases in the laboratory.[1–7] In generally, carbon materials, metal oxides, conductive polymers and composite substances can be applied to supercapacitor electrodes. In particularly, it is important that the electrode materials with special microstructure, unique morphology, suitable particle size and the matched pore size as well as the desirable surface physicochemical characteristics possess the superior electrochemical properties in factual applications.[8–11] Up to now, various porous carbon materials, especially activated carbons, have been extensively studied for supercapacitors because of their large surface areas, good electronic conductivities, low matrix resistivity, ideal electric double layer mechanism, stable physicochemical properties and long cycle life.[12,13]

Currently, porous activated carbon materials were synthesized by pyrolysis and/or chemical or physical activation of the carbonaceous precursor, such as polymeride based carbon, spent coffee grounds, beer yeast and mesoporous carbon microspheres.[8,14–16] KOH is known as one of the most effective activating agent for the preparation of the porous activated carbons. KOH-treated activated carbons are prepared by pyrolysis of mixtures of carbon precursor/alkaline hydroxide under the inertia atmosphere, which possess the higher specific surface area and pore volume than carbon precursor without KOH activation. Compared with physical activation (carbon oxide and water vapor activation), KOH chemical activation could trigger a significant difference between the surface topography of carbon precursor and as-obtained carbon products and destruction of the nature morphology.[15,17]

Biomass and by-products of crops have been extensively used as the precursor for the preparation of various carbon materials because of their advantages of low cost, easy preparation and may mimic the inherent structure of the natural materials.[18] In our previous work, the wasted tea-leaves,[19] pomelo peel,[20] and celtuce leaves[21] have been used as the precursor for the preparation of carbon materials, the as-prepared porous carbons all exhibits good capacitive performance in KOH aqueous electrolyte, with the specific capacitance over 330 F g^{-1} and excellent cycle stability. Interconnected carbon nanosheets with superior capacitive performance were prepared by KOH activation of the hydrothermal product of hemp bast fiber.[22] Zhang and co-authors prepared activated carbon materials from various pollens by hydrothermal condition followed by an industry KOH activation step without carbonization process.[23] Perhaps most importantly, KOH treated porous carbon would gradually

Laboratory of Clean Energy Chemistry and Materials, State Key Laboratory of Solid Lubrication, Lanzhou Institute of Chemical Physics, Chinese Academy of Sciences, Lanzhou 730000, P. R. China. E-mail: jwlang@licp.cas.cn; Fax: +86 931 4968055; Tel: +86 931 4968055

Published on 30 March 2015. Downloaded by Michigan State University on 25/01/2016 01:14:11.

omit the carbonization process, and the low energy-consuming process is propitious for practical application.

SL is a traditional Chinese drug, which reputed for its prevention of, and as a remedy against, pharyngitis. It has also been used for the treatment of tussis and constipation since ancient times in China. Usually, the waste SL is discarded as a waste after usage. Waste SL are common waste and also widely available. More importantly, the SL possess high water absorption, and the wasted SL have loosely packed microstructure, which can help them fully mix and react with activating agents such as KOH, to achieve high specific surface area and enlarge the pore size. However, the potential applications of wasted SL in energy storage may have been overlooked.

Thus, in this work, two nanoporous carbons were prepared from SL by simple hydrothermal condition and followed by KOH activation step, and studied the difference in structure and electrochemical performance of the obtained carbons prepared with and without carbonization process. The result showed that the as-obtained two carbon materials exhibit different surface topography *via* the SEM measurements. But both carbons show extremely high specific surface area (2589 $m^2 g^{-1}$ for AC-1, 2660 $m^2 g^{-1}$ for AC-2) and display remarkable electrochemical performance with substantially high specific capacitance (312.1 F g^{-1} for AC-1, 354.3 F g^{-1} for AC-2), good rate capability and extraordinary cycling stability, which can be attributed to its unique porous structure with a high SSA and abundant porosity. Moreover, a fully packaged symmetric supercapacitor can work in a wider voltage window of 1.7 V without any significant capacitance fade during 3000 cycles, the highest specific capacitance of 47.8 F g^{-1} and energy density of 18.5 W h kg^{-1} are demonstrated.

2 Experimental section

2.1 Preparation of the AC-1 and AC-2 carbon materials

The dried SL was firstly marinated in boiling water until it is swelled. 5 g of swelled SL was placed in a 250 ml stainless steel autoclave which was sealed and heated at 180 °C for 12 h and cool to room temperature. The resulting carbonaceous solid was filtered, and washed with ultra-pure water before vacuum freeze drying. The as-obtained substance was denoted as biochar. The biochar directly mix with a certain weight of KOH in aqueous solution at 80 °C for 24 hours *via* vigorous stirring. Subsequently, as-obtained mixtures were heated at 800 °C for 1 h under the argon atmosphere. After being cooled down to room temperature in flowing argon flow, the product was neutralized by the 1 M HCl solution until a pH value of 7 was reached. Finally, as-prepared activated carbon (denoted as AC-1) was filtered, washed with ultra-pure water, and dried at 60 °C in ambient for 10 h.

The biochar was carbonized at 600 °C for 2 h in a horizontal tube furnace, and KOH activation of the pyrolysis products at 800 °C for 1 h in the horizontal tube furnace with the same of KOH weight-ratio to the AC-1 process. As-obtained carbon material was named as AC-2. The obvious difference for AC-1 and AC-2 is carbonization step in preparation process: AC-1 without carbonization step, AC-2 with carbonization step.

2.2 Structural characterization

The morphology and microstructure of the obtained products were investigated using a field emission scanning electron microscope (FE-SEM, JSM-6701F). The chemical compositions of the both carbon samples were analyzed by Fourier transformation infrared spectroscopy (FTIR) using a Bruker IFS66V FTIR spectrometer. Nitrogen adsorption–desorption isotherm measurements were performed on a Micromeritics ASAP 2020 volumetric adsorption analyzer at 77 K. Prior to the adsorption experiments, all X-AC sample were adopted degassing process at 200 °C for 4 h to eliminate the surface gaseous contaminants. The Brunauer–Emmett–Teller (BET) method was utilized to calculate the specific surface area of each sample and the pore-size distribution was derived from the adsorption branch of the corresponding isotherm using the Barrett–Joyner–Halenda (BJH) method. The total pore volume was estimated from the amount adsorbed at a relative pressure of $P/P^o = 0.99$. The surface functionality of AC samples was analyzed on a Perkin-Elmer PHI-5702 multifunctional X-ray photoelectron spectroscope (XPS, physical electronics, USA) using Al Kα radiation of 1486.6 eV as the excitation source.

2.3 Electrode preparation and electrochemical measurements in three-electrode system

The working electrodes were prepared following the method: 80 wt% of powder active material was mixed with 7.5 wt% of acetylene black (>99.9%) and 7.5 wt% of conducting graphite in an agate mortar until a homogeneous black powder was obtained. To this mixture, 5 wt% of poly(tetrafluoroethylene) was added with a few drops of ethanol. After briefly allowing the solvent to evaporate, the resulting paste was coated in nickel gauze. The electrode assembly was dried for 16 h at 80 °C in air, and then was pressed at 10 MPa. Each carbon electrode contained about 8 mg of electroactive material for the electrochemical performance tests.

All the electrochemical measurements of each as-prepared electrode were carried out by an electrochemical working station (CHI660D, Shanghai, China) using a three-electrode system in 2 M KOH and 1 M $NaNO_3$ electrolytes at room temperature. A platinum sheet electrode and a saturated calomel electrode served as the counter electrode and the reference electrode, respectively. Galvanostatic charge/discharge (GCD), cyclic voltammetry (CV) and electrochemical

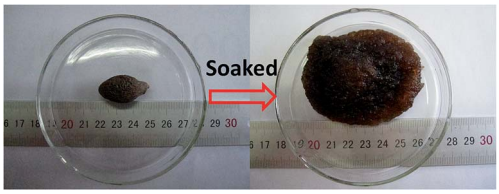

Fig. 1 Images of the dried SL before and after soaked in boiling water.

 This journal is © The Royal Society of Chemistry 2015

Published on 30 March 2015. Downloaded by Michigan State University on 25/01/2016 01:14:11.

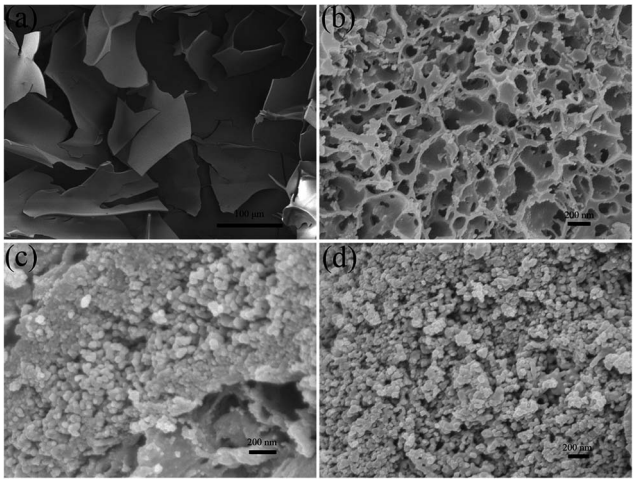

Fig. 2 SEM image of the porous carbon materials: SL based biochar (a); AC-1 (b); SL based biochar after carbonization (c); AC-2 (d).

impedance spectroscopy (EIS) measurements were performed to investigate the electrochemical performances of the as-prepared AC-1 and AC-2 electrode. The corresponding specific capacitance was calculated from:

$$C(\mathrm{F\ g^{-1}}) = I/[(\mathrm{d}E/\mathrm{d}t) \times m] \approx I/[(\Delta E/\Delta t) \times m] \quad (1)$$

where C is the specific capacitance, I is the constant discharging current, $\mathrm{d}E/\mathrm{d}t$ indicates the slope of the discharging curves, and m is the mass of the corresponding electrode material.

2.4 Electrochemical measurements in two-electrode system

Four symmetric supercapacitors were fabricated. The electrodes were prepared using nickel foam as the current collectors; each electrode contained 8 mg of electrochemical active material. Before assembling the supercapacitor configuration, carbon electrodes and cloth separator were immersed in aqueous electrolyte to make electrolyte ions homogeneously diffuse into the porous carbon materials. The cathode and anode electrode were pressed together and separated by a porous nonwoven cloth separator. The electrochemical measurements of the symmetric supercapacitor were carried out in 2 M KOH and 1 M $NaNO_3$ aqueous electrolyte using the electrochemical working station in a two-electrode cell at room temperature.

The value of specific capacitance was calculated from discharge process according to the following equation:

$$C_{\mathrm{T}}(F/g) = \frac{I \times \Delta t}{\Delta E \times m} \quad (2)$$

where I in A is the constant discharging current; Δt in s is the discharge time; ΔE in V is the potential window during the discharge process after IR drop; and m in g is the total mass of the two-electrode materials.

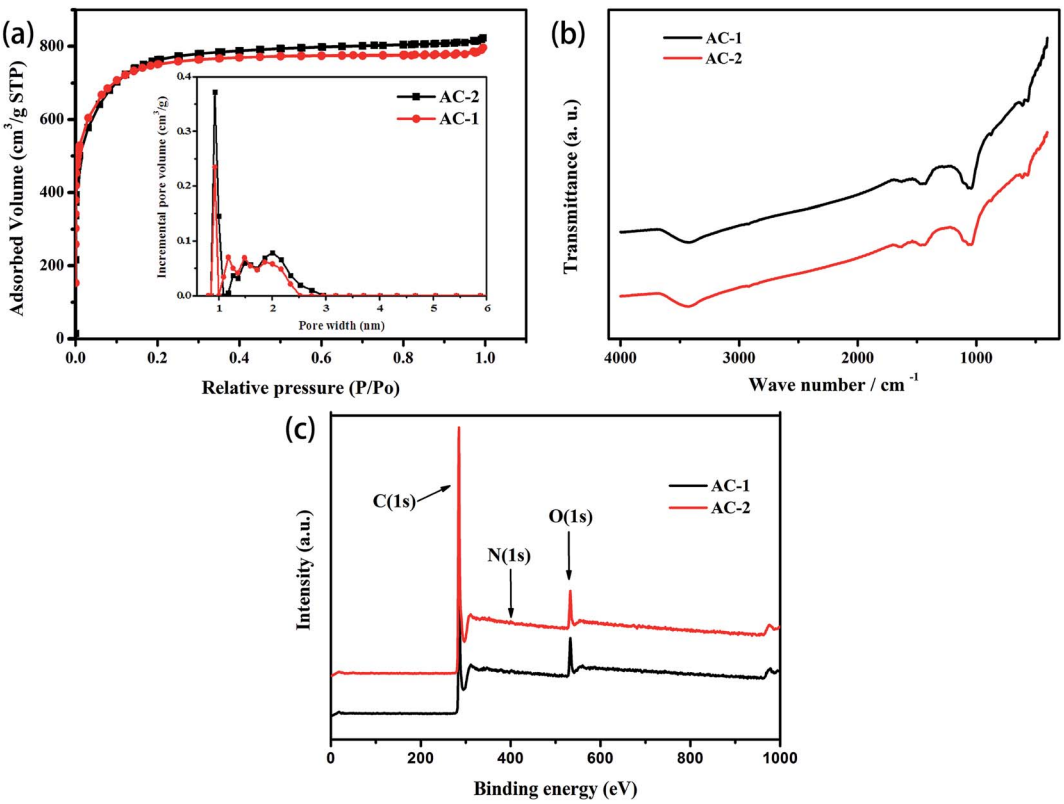

Fig. 3 (a) Nitrogen adsorption isothermal curves of AC-1 and AC-2 samples, the inset is the pore size distributions of the corresponding materials, which are calculated by DFT method; (b) the FTIR spectra of the AC-1 and AC-2 samples; (c) the XPS spectra of AC-1 and AC-2 samples.

Published on 30 March 2015. Downloaded by Michigan State University on 25/01/2016 01:14:11.

Specific energy density and power density are very important performance parameters of supercapacitor cell, which can be defined as follow (based only on the total mass of both electrodes):

$$E(\mathrm{W\ h\ kg^{-1}}) = \frac{0.5 C_T V^2}{3.6}$$
$$P(\mathrm{W\ kg^{-1}}) = \frac{E \times 3600}{t} \quad (3)$$

where V in V is the voltage change during the discharge process after IR drop, and t in s is the discharge time.

3 Discussion and result

3.1 Structure and morphology

Fig. 1 shows the picture of dried SL before and after soaked in boiling water. This is an interesting phenomenon that the volume of SL expand significantly after soaked in boiling water, it is attributed to the high water absorption of the SL. Fig. 2 shows some typical microstructures of the activated carbon materials used in this study. The chemical activation of carbonaceous precursor with hydroxides has recently been of great efforts due to the highly developed porosity of the prepared activated carbons.[24] It is noteworthy that the SL based biochar after vacuum freeze drying displays the micrometer-sheets and cross linked structure (Fig. 2a). The morphology of AC-1 sample (Fig. 2b) (without carbonization process and directly chemical activation by KOH) exhibits cross linked and hole-like structure. However, the SL based biochar after carbonization and activation process shows dozens of nanometer microspheres on the surface of AC-2 sample (Fig. 2c and d). It is obvious that the carbonization process leaded to large morphology difference between AC-1 and AC-2, the particle size of AC-2 is smaller than that of AC-1.

The porosity and BET surface area of the AC-1 and AC-2 samples were studied using nitrogen adsorption–desorption experiments (Fig. 3a). As shown in the inset of Fig. 3a, the pore-size of both carbon samples are estimate to less than 3 nm in a

Table 1 The elemental compositions, the specific surface area, pore structures, and specific capacitance of the AC-1 and AC-2 samples

Sample	C at%	O at%	N at%	BET specific surface area ($m^2\ g^{-1}$)	BJH pore volume ($cm^3\ g^{-1}$)	BJH pore size (nm)	Specific capacitance in KOH electrolyte ($F\ g^{-1}$)	Specific capacitance in $NaNO_3$ electrolyte ($F\ g^{-1}$)
AC-1	90.95	8.26	0.79	2589	1.21	2.78	312.1	255.5
AC-2	92.27	7.12	0.61	2660	1.258	3.321	354.3	320.8

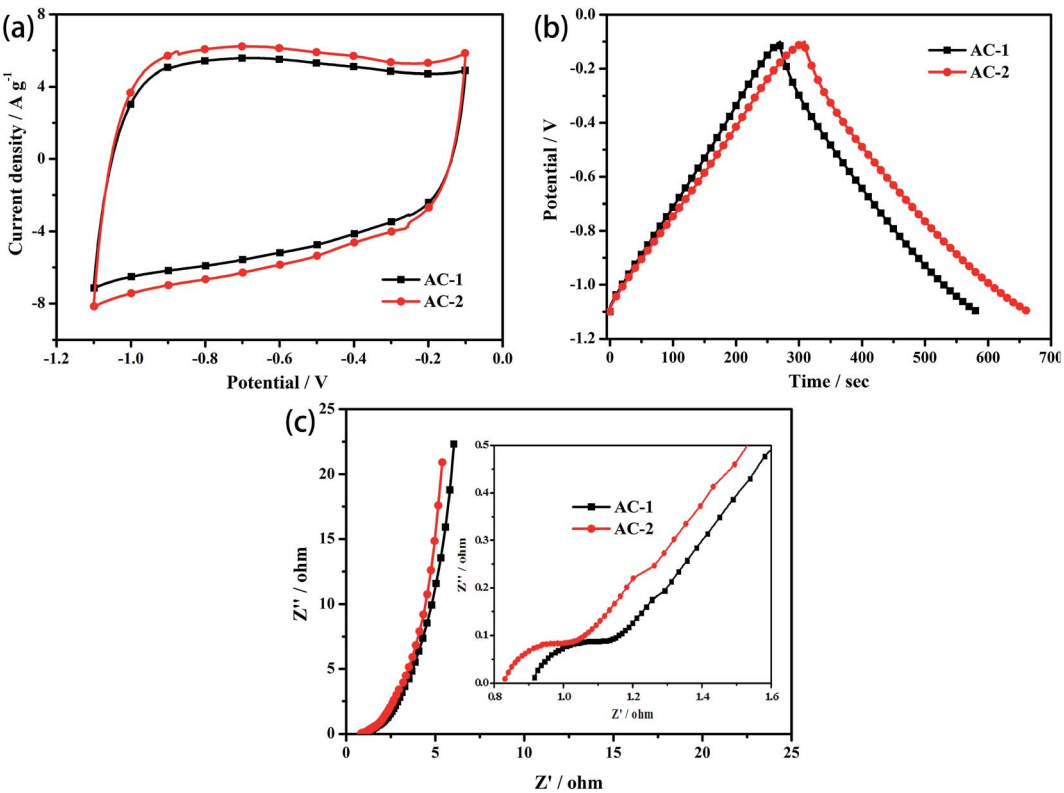

Fig. 4 Electrochemical performances of the AC-1 and AC-2 electrode in 2 M KOH electrolyte in three-electrode cell: (a) CV curves at sweep rate of 20 mV s^{-1}; (b) charge–discharge curves at the current density of 1 A g^{-1}; (c) complex-plane impedance plots of the AC-1 and AC-2 electrode, the inset is the high frequency regions.

 This journal is © The Royal Society of Chemistry 2015

Published on 30 March 2015. Downloaded by Michigan State University on 25/01/2016 01:14:11.

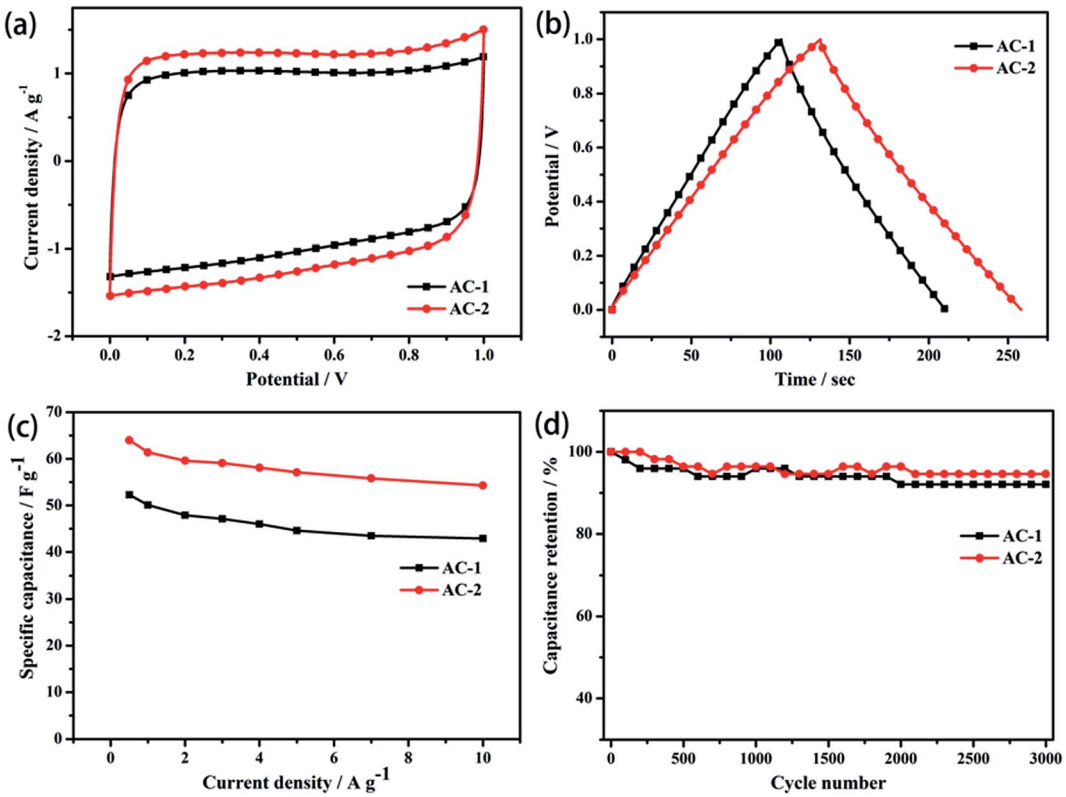

Fig. 5 Electrochemical performances for both symmetric supercapacitor in KOH electrolyte: (a) CV curves at sweep rate of 20 mV s^{-1}; (b) charge–discharge process at the current density of 0.5 A g^{-1}; (c) dependence of specific capacitance on discharge current density; (d) capacitance retention at the current density of 2 A g^{-1} after 3000 cycle numbers.

diameter, a peak about 1 nm can be found in the micropores region and parts of mesopores. The adsorption isotherms of AC-1 and AC-2 carbon materials display a type-I curve with a steep increase at low relative pressure and followed by a plateau at high relative pressure, suggesting the microporous nature dominates. The AC-1 sample exhibits the BET surface area of 2589 m^2 g^{-1}, pore volume of 1.21 cm^3 g^{-1} and BJH average pore width of 2.78 nm, whereas the BET surface area, pore volume and BJH average pore width of AC-2 sample are 2660 m^2 g^{-1}, 1.258 cm^3 g^{-1} and 3.321 nm, respectively. The effective pore size and high specific surface area are beneficial to the accesses of electrolyte ion into the pores and ionic transportation.[25] Generally, the higher pore volume and BET specific surface area, the higher electrochemical capacitive behavior was obtained.

As we know, besides surface area and pore characteristics, chemical contribution also plays an important role in determining the capacitive performance of porous carbon materials. The amount of stored energy of carbon-based supercapacitors can be obviously enhanced through pseudo-faradic reactions of active groups (such as oxygen-, nitrogen- and boron-functionalities) on the surfaces of carbon.[26–28] Therefore, the FTIR measurements were employed to monitor chemical composition on the surface of the AC-1 and AC-2 samples. It can be seen from Fig. 3b, the FTIR spectra shows the presence of C–O in carbonyl (ν_{C-O} at 1042 cm^{-1}), C=O in carboxylic acid and/or carbonyl moieties ($\nu_{C=O}$ at 1639 cm^{-1}) as well as C=C stretching deformation of a honeycomb carbon network at 1441 cm^{-1} for the surface functionalities of AC-1 and AC-2 samples.[29] From XPS test, it is confirmed that O and N were exist on the surface of AC samples, indicating a significant amount of O- and N-containing C groups were formed meantime. Actually, these O- and N-containing functional groups can make effects on the electrochemical capacitive behaviors.

Table 1 summarizes the elemental compositions, the specific surface area, pore structures, and specific capacitance of the AC-1 and AC-2 samples. It is obvious that the carbonization treatment not only leaded to the slight increase in the specific surface area, pore volume and average pore size, but also leaded to the slight decrease in the O and N compositions.

3.2 Electrochemical test for carbon electrodes in KOH aqueous electrolyte in three-electrode cell

CV and chronopotentiometry measurements were employed to evaluate the electrochemical properties and to calculate the specific capacitance of as-prepared AC-1 and AC-2 electrode. Fig. 4a shows the CV curves of the AC-1 and AC-2 electrodes in 2 M KOH aqueous electrolyte at sweep rate of 20 mV s^{-1}. It can be seen that the CV curves were both closed to rectangular shape, indicating of well capacitive performance for both of activated carbon materials with high specific surface area and microporous *via* KOH activation.

Published on 30 March 2015. Downloaded by Michigan State University on 25/01/2016 01:14:11.

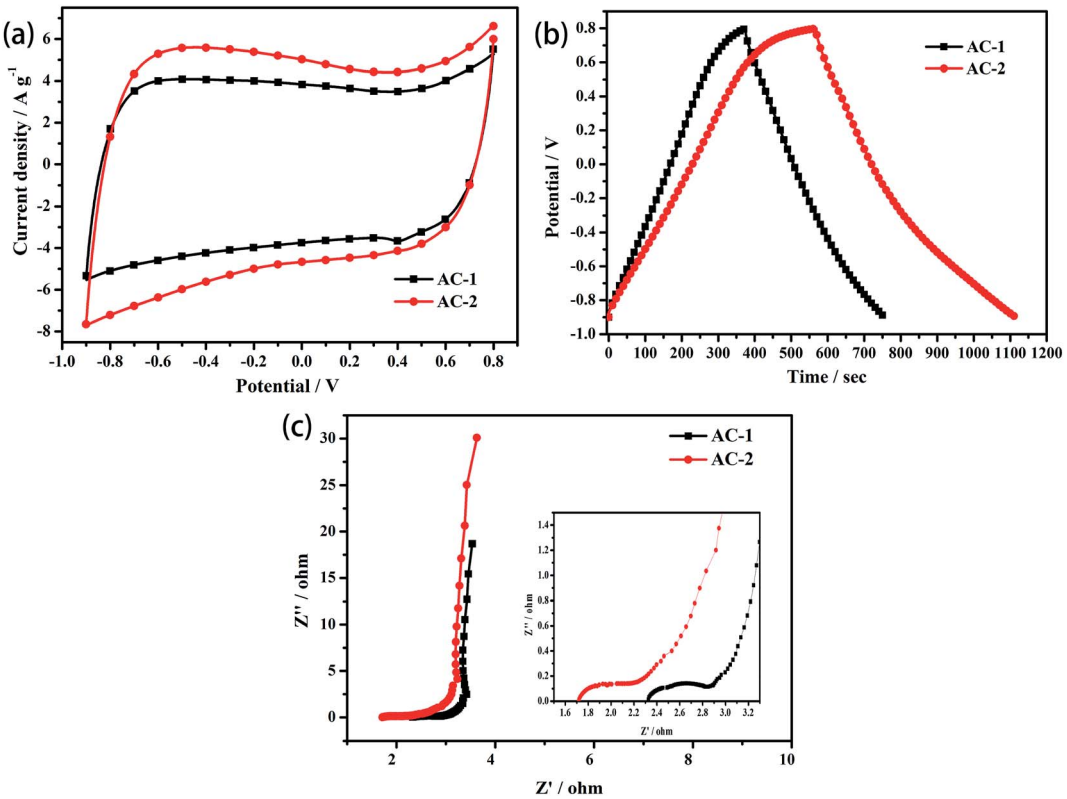

Fig. 6 Electrochemical performances of the AC-1 and AC-2 electrode in 1 M $NaNO_3$ electrolyte in three-electrode cell: (a) CV curves at sweep rate of 20 mV s^{-1}; (b) charge–discharge curves at the current density of 1 A g^{-1}; (c) complex-plane impedance plots of the AC-1 and AC-2 electrode, the inset is the high frequency regions.

However, a pair of low and broad peaks also appeared in the CV curves, indicating superimposed and reversible faradaic surface redox reactions, behaving as pseudo-capacitance. As we know, the O- and N-containing functional groups are able to provide some pseudo-faradaic contribution in electrolyte through redox reactions of these functionalities. So, the pseudo-capacitance is attributed to the O- and N-containing functional groups.

The charge–discharge curves of the AC-1 and AC-2 electrode measured in 2 M KOH at a current density of 1 A g^{-1} in operating potential between −1.1 and −0.1 V are shown in Fig. 4b. It is clear seen that the shape of the charge–discharge curves of the AC electrodes are closely linear and show a typical triangle symmetrical distribution, indicating a good double layer capacitive property. The specific capacitance values for AC-1 and AC-2 electrodes are 312.1 F g^{-1} and 354.3 F g^{-1}, respectively, suggesting that the electrochemical capacitances of the biochar are remarkably enhanced by the KOH activation.

The complex plane plots of the AC impedance spectra in KOH electrolyte for the two electrodes are shown in Fig. 4c. For each sample, there is a semi-circle intersecting the real axis in the high frequency range, and the plot transforms to a vertical line with decreasing frequency. As the plots show, the AC-2 electrode has smaller internal resistance (from the point intersecting with the real axis in the range of high frequency) and decreased faradic charge transfer resistance (semicircle) than that of the AC-1 electrode. These observations are strongly correlated with the increase of the total capacitance. In addition, both the two plots show a Warburg angle higher than 45°, indicating the suitability of the AC as the electrode materials for supercapacitors.

3.3 Symmetric supercapacitors in KOH aqueous electrolyte

Panels a and b in Fig. 5 shows the electrochemical performances of symmetric supercapacitors based on AC-1 and AC-2 carbon electrode in KOH electrolyte for a fixed potential range of 0–1 V. Both symmetric supercapacitors show nearly rectangular CV profile, which are characteristics for capacitors with low contact resistance.[30,31] The fast current response can be clearly found in positive and negative electrodes, and the leveled current separation between leveled anodic and cathodic currents is large, suggesting the good electrochemical capacitive behavior. Furthermore, the charge–discharge curves of the two cell capacitors exhibit good linearity and equilateral triangle, indicating a purely electrochemical double-layer capacitive behavior.[32,33] The specific capacitance of the cell supercapacitors based on AC-2 and AC-2 calculated according to the formula (2) are 53 F g^{-1} and 64 F g^{-1}, respectively.

Fig. 5c shows the change in the specific capacitance as a function of the discharge current density ranging from 0.5 to 10 A g^{-1}. The highest specific capacitance of 53 F g^{-1} and

 This journal is © The Royal Society of Chemistry 2015

Published on 30 March 2015. Downloaded by Michigan State University on 25/01/2016 01:14:11.

64 F g^{-1} for AC-1 and AC-2 based symmetric supercapacitors were obtained at the current density of 0.5 A g^{-1}, respectively. When the current density as high as 10 A g^{-1}, the capacitance retention of these electrodes are 80.9% and 84.8%, respectively. The excellent capacitive behaviors confirmed that the AC-1 and AC-2 carbon materials with oxygen-enriched surface and high specific surface area hold superior supercapacitive. The excellent cycle stability of the symmetric supercapacitor cell was demonstrated *via* running a constant current charge–discharge process. As shown in Fig. 5d, after charge–discharge the capacitors between 0 and 1 V during 3000 cycles at the current density of 2 A g^{-1}, about 92.1% and 94.6% of the initial specific capacitances still are retained for the AC-1 and AC-2 based symmetric supercapacitors, respectively, indicating of the cell capacitors exhibit long-term cycle stability and good electrochemical reproducibility.

3.4 Electrochemical test for carbon electrodes in $NaNO_3$ aqueous electrolyte in three-electrode cell

Fig. 6a shows the CV curves of the AC-1 and AC-2 electrodes between −0.9 and 0.8 V (*vs.* SCE) in 1 M $NaNO_3$ aqueous electrolyte at sweep rate of 20 mV s^{-1}. It can be seen that the CV curves were both also closed to rectangular shape, indicating of well capacitive performance for both of activated carbon materials. Meanwhile, a pair of low and broad peaks also could be seen in the CV curves, indicating superimposed and reversible faradaic surface redox reactions, behaving as pseudocapacitance. As seen in Fig. 6b, the shape of the charge–discharge curves of the AC electrodes are closely linear and show a typical triangle symmetrical distribution in $NaNO_3$ electrolyte, indicating a good double layer capacitive property. The specific capacitance values for AC-1 and AC-2 electrodes are 255.5 F g^{-1} and 320.8 F g^{-1}, respectively. The complex plane plots of the AC impedance spectra in $NaNO_3$ electrolyte for the two electrodes are shown in Fig. 6c. As the plots show, the AC-2 electrode also possesses smaller internal resistance and decreased faradic charge transfer resistance than that of the AC-1 electrode in $NaNO_3$. These observations are also strongly correlated with the increase of the total capacitance.

3.5 Symmetric supercapacitors in $NaNO_3$ aqueous electrolyte

To further explore such new carbon-based supercapacitors, it is very necessary to study their electrochemical performances in neutral aqueous electrolyte (such as $NaNO_3$). Fig. 7a shows the two cell capacitor based on AC-1 and AC-2 at the scan rates of 20 mV s^{-1}. Totally, it can be seen that the CV area of supercapacitor based on AC-2 electrodes is also slightly higher than that of the cell capacitor based on AC-1. Fig. 7b shows galvanostatic charge–discharge curves of AC-1 and AC-2 cell capacitor at the current density of 0.5 A g^{-1}, the longer charging time of the AC-2 cell capacitor suggests that the carbonization process

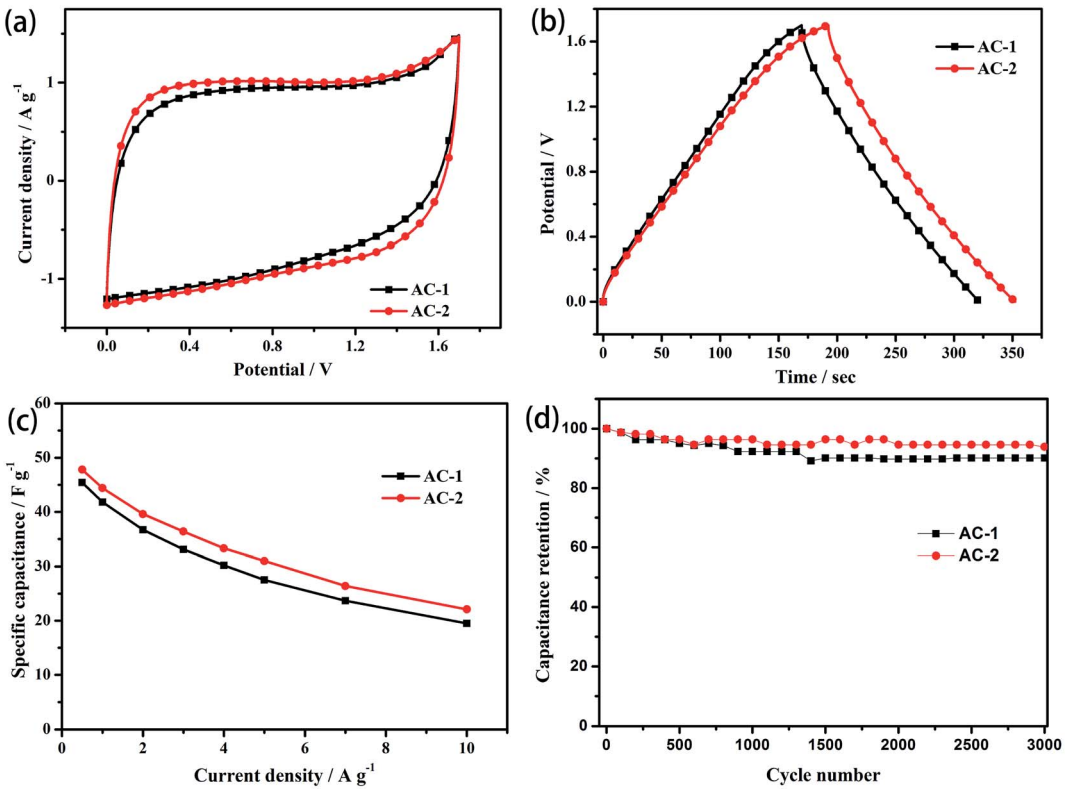

Fig. 7 Electrochemical performances for both of symmetric supercapacitor in $NaNO_3$ electrolyte: (a) CV curves at sweep rate of 20 mV s^{-1}; (b) charge–discharge process at the current density of 0.5 A g^{-1}; (c) dependence of specific capacitance on discharge current density; (d) capacitance retention at the current density of 2 A g^{-1} after 3000 cycle numbers.

Published on 30 March 2015. Downloaded by Michigan State University on 25/01/2016 01:14:11.

can slightly increase the specific capacitance of the obtained carbon electrode. The specific capacitance is shown as a function of the current density in Fig. 7c. The specific capacitances of AC-1 cell capacitor were 45.4, 41.8, 36.7, 33.1, 30.2, 27.5, 23.7 and 19.5 F g^{-1} at the current density of 0.5, 1, 2, 3, 4, 5, 7, and 10 A g^{-1}, respectively. In contrast, AC-2 cell capacitor shows the specific capacitance of 47.8, 44.4, 39.6, 36.4, 33.3, 31, 26.4 and 22.1 F g^{-1} for the same current density, respectively. The decrease in the specific capacitance at high current density can be attributed to the increase of the potential drop due to the conductivity of the carbon materials, restraining electrolyte ion transport between the electrolyte solutions and the active sites of the electrodes.[34] The cycling capability tests over 3000 cycles for both cell capacitors at a current density of 2 A g^{-1} were carried out in the potential windows ranging from 0 to 1.7 V. Electrochemical stability of two symmetry supercapacitor is depicted in Fig. 7d. After 3000 cycles, the capacitance retention of the two cell capacitors maintains 90.1% and 93.9% of the initial capacitance, respectively. We believed that the suitable porous structure and the oxygen functionality groups were in favor of the absorption and transport of electrolyte ions through the porous channels within the AC materials.

3.6 The difference between AC-1 and AC-2

As shown in Table 1, the two carbon samples have the same pore structures, but AC-2 sample possess higher specific surface area, higher specific pore volume, larger average pore size. As the high-surface-area is still predominant factor for electrode materials for supercapacitors, the higher specific capacitance of AC-2 is reasonable. Moreover, it is obvious that the particle size of AC-2 is smaller than that of AC-1. Small crystal size and high porosity of AC-2 could enlarge the electrolyte/electrode contact area and shorten the diffusion distance of electrolyte ion among the AC particles, thereby being favorable diffusion kinetics for electrons and electrolyte ions. Consequently, the AC-2 sample displayed a high specific capacitance, fast rate performance and long-term cycling.

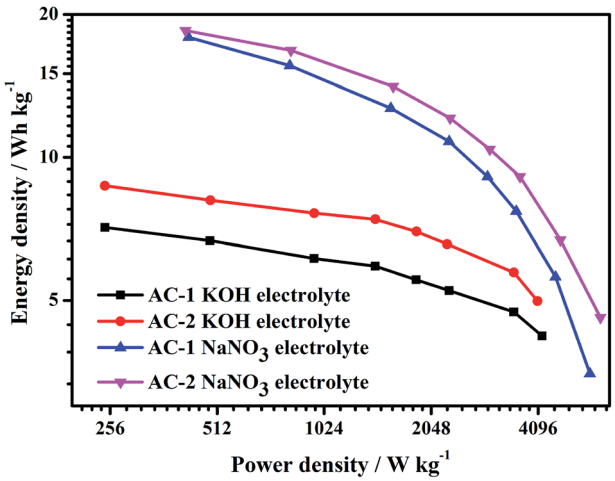

Fig. 8 Ragone plot for the symmetrical capacitors based on AC-1 and AC-2 in KOH and $NaNO_3$ electrolyte, respectively.

The important and crucial functionality of the electric storage devices are the energy and power density, which can determine their practical applications. Therefore, we calculated the values of the energy and power density *via* further performed the charge–discharge process at different current density of 0.5 A g^{-1} ~ 10 A g^{-1} for the four symmetric supercapacitors, the result shown in Fig. 8. Since energy stored is related to the square of voltage, and the voltage window in KOH and $NaNO_3$ electrolyte is 1.0 and 1.7 V, respectively, the energy density and power density of the supercapacitors in $NaNO_3$ electrolyte are much higher than those in KOH electrolyte. With the current density increasing, the energy density decreased while the power density increased for four symmetric supercapacitors. When the current density was 0.5 A g^{-1}, the energy density of the supercapacitors based on AC-1 in KOH and $NaNO_3$ electrolytes and the supercapacitors based on AC-2 in KOH and $NaNO_3$ electrolytes could reach up to 7.1, 17.9, 8.7 and 18.5 W h kg^{-1}, respectively. The energy densities of the four symmetric supercapacitors are as high as 4.2, 3.5, 5.0 and 4.6 W h kg^{-1} as the current density increased to 10 A g^{-1}, respectively.

4 Conclusions

In summary, two porous activated carbons with different surface topography were synthesized *via* the KOH activation the carbonaceous precursor of the dried SL under argon atmosphere without and with carbonization process. This treatment make for the nanometer pore size, higher specific surface area and abundant oxygen functional groups on the surface of the obtained carbon materials. Both the as-fabricated symmetric cell supercapacitors based on the AC-1 and AC-2 carbon materials exhibit excellent electrochemical performance in KOH and $NaNO_3$ aqueous electrolyte. Of great concern, the energy density of the symmetric supercapacitors with based on AC-1 and AC-2 carbon materials can reach to 17.9 W h kg^{-1} and 18.5 W h kg^{-1} in $NaNO_3$ aqueous electrolyte, respectively. Therefore, SL based porous carbon materials with different surface topography can be feasibly applied on carbon electrode for supercapacitors.

Acknowledgements

This work was supported by the National defense Basic Scientific Research Project of China (B1320133001) and the National Nature Science Foundations of China (21203223, 21201171).

References

1 M. R. Lukatskaya, O. Mashtalir, C. E. Ren and Y. Dall'Agnese, *Science*, 2013, **341**, 1502.
2 Y. H. Xiao, S. J. Liu, F. Li, A. Q. Zhang, J. H. Zhao, S. M. Fang and D. Z. Jia, *Adv. Funct. Mater.*, 2012, **22**, 4052.
3 H. J. Yu, Q. W. Tang, J. H. Wu, Y. Z. Lin, L. Q. Fan, M. L. Huang, J. M. Lin, Y. Li and F. D. Yu, *J. Power Sources*, 2012, **206**, 463.
4 X. B. Yan, J. T. Chen, J. Yang, Q. J. Xue and P. Miele, *ACS Appl. Mater. Interfaces*, 2010, **2**, 2521.

 This journal is © The Royal Society of Chemistry 2015

Published on 30 March 2015. Downloaded by Michigan State University on 25/01/2016 01:14:11.

5 W. W. Liu, X. B. Yan, J. W. Lang and Q. J Xue, *J. Mater. Chem.*, 2012, **22**, 8853.
6 J. W. Lang, X. B Yan, W. W Liu, R. T Wang and Q. J. Xue, *J. Power Sources*, 2012, **204**, 220.
7 S. Sahoo, S. Dhibar and C. K. Das, *eXPRESS Polym. Lett.*, 2012, **6**, 965.
8 G. Q. Zhang and S. T. Zhang, *J. Solid State Electrochem.*, 2009, **13**, 887.
9 J. L. Liu, J. Sun and L. Gao, *J. Phys. Chem. C*, 2010, **114**, 19614.
10 J. L. Liu, L. L. Zhang, H. B. Wu, J. Y. Lin, Z. X. Shen and X. W. Lou, *Energy Environ. Sci.*, 2014, **7**, 3709.
11 J. L. Liu, M. H. Chen, L. L. Zhang, J. Jiang, J. X. Yan, Y. Z. Huang, J. Y. Lin, H. J. Fan and Z. X. Shen, *Nano Lett.*, 2014, **14**, 7180.
12 J. W. Lee, J. Kim and T. Hyeon, *Adv. Mater.*, 2006, **18**, 2073.
13 A. G. Pandolfo and A. F. Hollenkamp, *J. Power Sources*, 2006, **157**, 11.
14 E. Frackowiak, G. Lota, J. Machnikowski, G. Vix-Gutera and F. Béguin, *Electrochim. Acta*, 2006, **51**, 2209.
15 M. G. Plaza, A. S. González, C. Pevida, J. J. Pis and F. Rubiera, *Appl. Energy*, 2012, **99**, 272.
16 W. Xiong, M. X. Liu, L. H. Gan, Y. K. Lv, Y. Li, L. Yang, Z. J. Xu, Z. X. Hao, H. L. Liu and L. W. Chen, *J. Power Sources*, 2011, **196**, 10461.
17 T. Tay, S. Ucar and S. Karagöz, *J. Hazard. Mater.*, 2009, **165**, 481.
18 Q. H. Liang, L. Ye, Z. H. Huang, Q. Xu, Y. Bai, F. Y. Kang and Q. H. Yang, *Nanoscale*, 2014, **6**, 13831.
19 C. Peng, X. B. Yan, R. T. Wang, J. W. Lang, Y. J. Ou and Q. J. Xue, *Electrochim. Acta*, 2013, **87**, 401.
20 C. Peng, J. W. Lang, S. Xu and X. L. Wang, *RSC Adv.*, 2014, **4**, 54662.
21 R. T. Wang, P. Y. Wang, X. B. Yan, J. W. Lang, C. Peng and Q. J. Xue, *ACS Appl. Mater. Interfaces*, 2012, **4**, 5800.
22 L. Zhang, F. Zhang, X. Yang, K. Leng, Y. Huang and Y. H. Chen, *Small*, 2013, **9**, 1342.
23 H. L. Wang, Z. W. Xu, A. Kohandehghan, Z. Li, K. Cui, X. H. Tan, T. J. Stephenson, C. K. Kingondu, C. M. B. Holt, B. C. Olsen, J. K. Tak, D. Harfield, A. O. Anyia and D. Mitlin, *ACS Nano*, 2013, **7**, 5131.
24 M. A. L. Ródenas, J. J. Juan, D. C. Amorós and A. L. Solano, *Carbon*, 2004, **42**, 1371.
25 W. Xiong, M. X. Liu, L. H. Gan, Y. K. Lv, Y. Li, L. Yang, Z. J. Xu, Z. X. Hao, H. L. Liu and L. W. Chen, *J. Power Sources*, 2011, **196**, 10461.
26 D. H. Jurcakova, M. Seredych, G. Q. Lu and T. J. Bandosz, *Adv. Funct. Mater.*, 2009, **19**, 438.
27 E. Frackowiak, G. Lota, J. Machnikowski, C. V. Guterl and F. Béguin, *Electrochim. Acta*, 2006, **51**, 2209.
28 D. W. Wang, F. Li, Z. G. Chen, G. Q. Lu and H. M. Cheng, *Chem. Mater.*, 2008, **20**, 7195.
29 L. F. Lai, H. P. Yang, L. Wang, B. K. The, J. Q. Zhong, H. Chou, L. W. Chen, W. Chen, Z. X. Shen, R. S. Ruoff and J. Y. Lin, *ACS Nano*, 2012, **6**, 5841.
30 R. B. Rakhi, D. Cha, W. Chen and H. N. Alshareef, *J. Phys. Chem. C*, 2011, **115**, 14392.
31 R. B. Rakhi, W. Chen, D. K. Cha and H. N. Alshareef, *J. Mater. Chem.*, 2011, **21**, 16197.
32 Y. Wang, Z. Q. Shi, Y. Huang, Y. F. Ma, C. Y. Wang, M. M. Chen and Y. S. Chen, *J. Phys. Chem. C*, 2009, **113**, 13103.
33 Y. Gao, Y. S. Zhou, M. Qian, X. N. He, J. Redepenning, P. Goodman, H. M. Li, L. Jiang and Y. F. Lu, *Carbon*, 2011, **51**, 52.
34 Y. H. Xiao, S. J. Liu, F. Li, A. Q. Zhang, J. H. Zhao, S. M. Fang and D. Z. Jia, *Adv. Funct. Mater.*, 2012, **22**, 4052.